COMMUNICATION

π-Conjugated Lewis Base: Efficient Trap-Passivation and Charge-Extraction for Hybrid Perovskite Solar Cells

Yuze Lin, Liang Shen, Jun Dai, Yehao Deng, Yang Wu, Yang Bai, Xiaopeng Zheng, Jiayu Wang, Yanjun Fang, Haotong Wei, Wei Ma, Xiao Cheng Zeng, Xiaowei Zhan, and Jinsong Huang**

In both inorganic and organic semiconducting materials, trap states and localized electronic states in the forbidden gap caused by material imperfections are one of the main limiting factors to high performance optoelectronic devices, such as solar cells, ultrafast photodetectors, field effect transistors, light-emitting diodes, among others. Suppressing these trap states in semiconductor thin films through a simple and efficient approach is thus critical to the enhancement of optoelectronic device performance. A new generation of photovoltaic materials, namely, organic–inorganic halide perovskites (OIHPs),[1] have been shown to possess unique defect tolerant properties, which can give rise to a very long carrier diffusion length, significantly longer than the optical absorption length in both single crystals and polycrystalline films. The power conversion efficiency (PCE) of solar cells based on OIHPs has skyrocketed in the past few years,[2–7] in part due to negligible charge recombination in the grain interior.[5,8–10] On the other hand, the polycrystalline films still have several orders magnitude higher density of traps than in single crystals, suggesting the presence of a large density of charge traps at grain boundaries (GBs) or the film surface.[11–13] A recent direct optical study revealed strong surface recombination in single crystalline $CH_3NH_3PbI_3$ ($MAPbI_3$), the most studied OIHP material thus far for solar cells.[14] Thus, lowering the carrier recombination at the GBs of perovskite polycrystalline thin films, and contacts between perovskite active layer and electrodes is critical to achieving high efficiency perovskite solar cells. To date, many research efforts have been made to enlarge grains of the perovskite polycrystalline films for reducing the total GB area;[15–19] for example, large-aspect-ratio (up to 7.9) polycrystalline perovskite grains have been grown on a nonwetting surface,[15] resulting in over tenfold reduced charge recombination in the devices. Now that photogenerated carriers can flow through perovskite films with negligible charge recombination, minimization of the charge recombination at the contacts becomes increasingly important to produce highly efficient perovskite solar cells. Thus, efficient passivation techniques to lower the recombination at perovskite film surfaces are critically needed for achieving very high device efficiency.[20–24]

Due to the low thermal stability of $MAPbI_3$, methylammonium iodide can be lost from the crystal; unavoidable thermal annealing (usually at temperatures above 80 °C) in the deposited process of $MAPbI_3$ film can cause nonstoichiometry in composition and also decompose $MAPbI_3$ to PbI_2 on the surface and at the GBs of polycrystalline films,[25–27] where unsaturated or under-coordinated Pb ions are most frequently found. The theoretical modeling and experimental studies have shown that these under-coordinated Pb atoms, or/and Pb clusters in some cases, can act as the electronic trap states within the perovskite material[28,29] and also as one of main surface traps that greatly limit the performance of $MAPbI_3$-based devices. The under-coordination of the Pb atom can result in the formation of net positive charges on the atom, which would then create favorable conditions for coordination or bond formation with electron-rich Lewis bases.[22,24]

Herein, for the first time, we introduce a π-conjugated Lewis base with n-type semiconductor property to the $MAPbI_3$ based solar cells as an interlayer between $MAPbI_3$ and cathode. The π-conjugated Lewis base is essentially a type of organic semiconducting molecules attached with Lewis base blocks. It has multifunction that can combine trap-passivation and charge-extraction, which can increase both photovoltage and photocurrent. The Lewis base can effectively passivate the Lewis acid traps (e.g., under-coordinated Pb ions and Pb clusters) on the surface and at the GBs of $MAPbI_3$, and the n-type π-conjugated material possesses chemical properties that promote electron extraction and electron transport. The principle of engineering $MAPbI_3$ surface by π-conjugated Lewis base is illustrated in **Figure 1**a, where the formation of Lewis adducts (Figure 1b) can passivate the trap states (Figure 1c) of $MAPbI_3$ polycrystalline films. The organic n-type π-conjugated molecules can

Dr. Y. Lin, Dr. L. Shen, Y. Deng, Dr. Y. Bai, X. Zheng, Dr. Y. Fang, Dr. H. Wei, Prof. J. Huang
Department of Mechanical and Materials Engineering and Nebraska Center for Materials and Nanoscience
University of Nebraska-Lincoln
Lincoln, NE 68588, USA
E-mail: jhuang2@unl.edu
Dr. J. Dai, Prof. X. C. Zeng
Department of Chemistry
University of Nebraska-Lincoln
Lincoln, NE 68588, USA
Y. Wu, Prof. W. Ma
State Key Laboratory for Mechanical Behavior of Materials
Xi'an Jiaotong University
Xi'an 710049, China
J. Wang, Prof. X. Zhan
Department of Materials Science and Engineering
College of Engineering
Key Laboratory of Polymer Chemistry and Physics of Ministry of Education
Peking University
Beijing 100871, China
E-mail: xwzhan@pku.edu.cn

DOI: 10.1002/adma.201604545

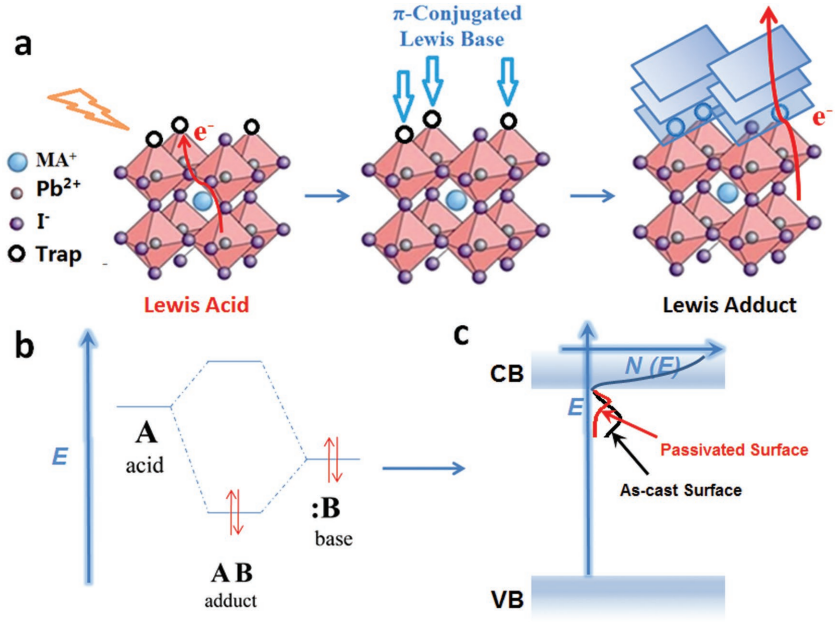

Figure 1. a) Schematic of the interaction of the π-conjugated Lewis base and Pb; b) Diagram depicting the formation of a dative covalent bond between two atoms; c) diagram of the passivation of trap states.

extract the electrons generated from $MAPbI_3$ and then transport them to the device cathode (Figure 1a). Finally, the $MAPbI_3$ based solar cells with low temperature solution-processed IDIC (a π-conjugated Lewis base: indacenodithiophene end-capped with 1.1-dicyanomethylene-3-indanone, molecular structure in Figure S1 in the Supporting Information and **Figure 2**a) layers result in a lower trap density, enhanced stabilized PCEs up to 19.5% with a higher open-circuit voltage (V_{OC}) of 1.11 V, more stable power output, and higher device stability compared with the control devices without IDIC layers.

Similar to several solution processed fullerene derivatives,[20,30–32] such as [6]-phenyl-C61-butyric acid methyl ester (PCBM), which are most commonly applied to planar heterojunction perovskite solar cells as electron-transporting layers (ETLs), the organic semiconductor IDIC[33] possesses the lowest unoccupied molecular orbital (LUMO: −3.9 eV) and the highest occupied molecular orbital (HOMO: −5.7 eV) energy levels (Figure S2, Supporting Information), and electron transporting property with an electron mobility of 1.1×10^{-3} cm^2 V^{-1} s^{-1}.[33] Thus, photo-induced electrons can transfer from $MAPbI_3$ to IDIC at the $MAPbI_3$/IDIC interface, and then can be collected efficiently by the device cathode. However, compared with isotropic packed PCBM, IDIC thin films show stronger self-aggregation and better π–π stacking, which can be supported by grazing incident wide-angle X-ray diffraction (GIWAXS) analysis of IDIC (Figure 2b,c) and PCBM (Figure S3, Supporting Information) neat films. From GIWAXS analysis, as-cast IDIC shows a longer π–π stacking coherence length of 3.5 nm than that of PCBM, which is ≈2.5 nm derived via the Scherrer equation.[34] The good π–π stacking of IDIC is also expected to give rise to a small energy disorder of electronic states, and then small V_{OC} loss in $MAPbI_3$/IDIC based solar cells.[35] The π–π stacking in the out-of-plane direction of the as-cast IDIC thin films is obviously stronger than that in the in-plane direction, which indicates that the IDIC molecules have predominantly face-on orientation. The vertical π–π stacking should facilitate the electron transport between $MAPbI_3$ and the cathode.

Furthermore, unlike the Lewis acid fullerenes which can passivate the Pb-I antisite defect,[21] the IDIC provides the Lewis base carbonyl (C=O) and cyano (C≡N), as electron-withdrawing end groups. Figure 2a shows an image of an electrostatic potential (ESP) surface computed using a density functional theory (DFT) method. The IDIC shows a planar π-conjugated main chain with a dominated continuous positive ESP, and the N and O atoms of IDIC concentrate negative charges. Thus the carbonyl and cyano groups are expected to passivate the under-coordinated Pb of $MAPbI_3$ through coordination between the Lewis acid and base.[36] To confirm the formation of Lewis adducts of Pb and O or N, we firstly measured the UV–vis absorption spectra of IDIC neat solution and IDIC: PbI_2 mixed solution. Generally, the formation of a coordination bond between metallic ions and organic ligands will change the conjugated structures of the chromophore, and then shift its absorption peaks.[37] IDIC in *N*,*N*-dimethyl formamide (DMF) solution exhibits broad absorption in the 400–700 nm region with two peaks at 496 and 636 nm (**Figure 3**a); IDIC: PbI_2 mixed in DMF solution shows obviously stronger and blue shifted absorption (two peaks at 485 and 611 nm) relative to IDIC neat solution, which indicates the existence of a relatively strong interaction between PbI_2 and IDIC. Then to further confirm the mechanism of interaction, the Fourier transform infrared (FTIR) spectroscopy measurement was conducted to analyze the IDIC powder and IDIC:$MAPbI_3$ blend. For the neat IDIC powder, the peaks of 1698 and 2215 cm^{-1} are assigned to the symmetric stretching vibrations of C=O bonds (ν(C=O)), and C≡N bonds (ν(C≡N)), respectively. To distinguish differences between IDIC and IDIC:$MAPbI_3$ easily, we normalized their FTIR maximum peak (1540 cm^{-1}) (Figure S4, Supporting Information) assigned to stretching vibrations of C=C bonds (aromatic nucleus), which is thus insensitive to Pb ions. The FTIR spectroscopy of the blended IDIC:$MAPbI_3$ powder shows weakened vibration strength for ν(C=O) and ν(C≡N) by 39% and 45%, respectively (Figure 3b), which confirmed the presence of interaction between $MAPbI_3$ and the C=O and C≡N of IDIC. It should be noted that the samples for absorption spectrum measurement were prepared at room temperature without any thermal annealing, which indicates that the passivation of $MAPbI_3$ by IDIC can bypass the widely used thermal annealing treatment in most of reported passivation processes.

The DFT calculation was also undertaken to investigate the function of IDIC, particularly the calculation of the density of states with and without IDIC on top of a $MAPbI_3$ surface with partial loss of MAI. As shown in Figure 3c, the deep trap

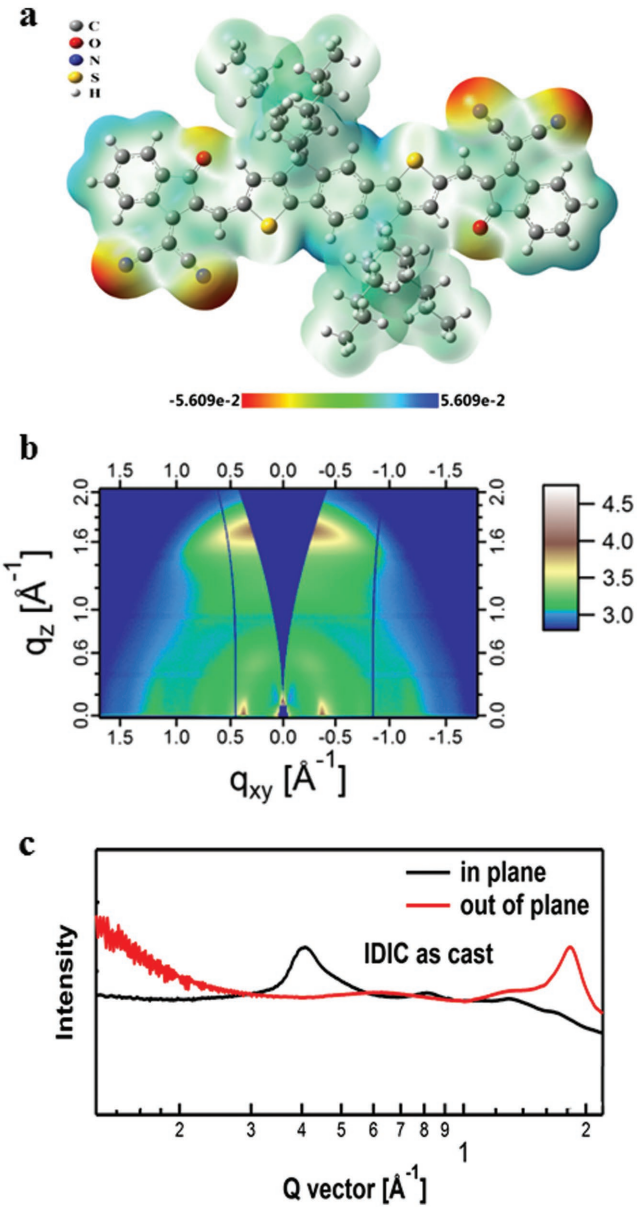

Figure 2. a) ESP of IDIC; b) 2D GIWAXS, and c) scattering profiles of in-plane and out-of-plane of IDIC film.

state (at −4.5 eV) induced by under-coordinated Pb clusters is lowered, and becomes much more shallow upon the adsorption of the C=O and C≡N of IDIC. We also found direct evidences for the passivation effect of IDIC by measuring the trap density of the devices with and without IDIC. The reduction of trap states in $MAPbI_3$ films by the passivation of the as-casted IDIC film was analyzed by using the thermal admittance spectroscopy (TAS) method. TAS is a well-established, effective technique for characterizing both shallow and deep defects, which has been broadly applied in understanding defects in thin films[38] and solar cells.[39] The energetic profile of trap density of states (tDOS) can be derived from the angular frequency dependent capacitance using the equation:[40]

$$N_T(E_\omega) = -\frac{V_{bi}}{qW}\frac{dC}{d\omega}\frac{\omega}{k_B T} \quad (1)$$

where C is the capacitance, ω is the angular frequency, q is the elementary charge, k_B is the Boltzmann's constant, and T is the temperature. V_{bi} and W are the built-in potential and depletion width, respectively, which were extracted from the Mott–Schottky analysis. The applied angular frequency ω defines an energetic demarcation:

$$E_\omega = k_B T \ln\left(\frac{\omega_0}{\omega}\right) \quad (2)$$

where ω_0 is the attempt–to–escape frequency. The trap states below the energy demarcation can capture or emit charges with the given ω and contribute to the capacitance. As shown in Figure 3d, there was a relatively large density of defect states in the order of 1×10^{18} to 1×10^{19} m^{-3} in the devices without IDIC passivation. The tDOS of traps with an energy depth of 0.33–0.45 eV decreased by one to two orders of magnitude after depositing IDIC layer on top of the $MAPbI_3$ films.

We further investigated the charge transfer between the $MAPbI_3$ films and IDIC by photoluminescence (PL). Here we confined the light attenuation region close to the surface of the perovskite layer by choosing the short wavelength excitation light of 532 nm which has a penetration length of 80 nm into $MAPbI_3$, much less than the thickness (i.e., ≈500 nm) of the perovskite films. The neat $MAPbI_3$ film showed the PL peak at 770 nm (**Figure 4**a), and then a PL quenching of $MAPbI_3$ by 87% was observed by the contacting of IDIC with $MAPbI_3$, larger than the observed quench ratio (70%)[20] by PCBM. This indicates IDIC yields higher efficiency of electron extraction from perovskite layers than PCBM. Meanwhile, $MAPbI_3$ covered with IDIC showed a 5 nm blue-shifted PL peak compared with the neat $MAPbI_3$ film, which agrees well with that expectation the IDIC can passivate the traps at the $MAPbI_3$ surface by filling the deep traps and/or shifted deep traps to shallow traps.[20] The time-resolved photoluminescence (TRPL) study of $MAPbI_3$ and $MAPbI_3$/IDIC films also revealed efficient charge extraction from $MAPbI_3$ to IDIC. Samples were excited with a 404 nm pulsed diode laser with a pulse width of 45 ps. As shown in Figure 4b, the neat $MAPbI_3$ film had a decay time of 96 ns calculated with a single exponential decay function fitting. The quick portion of the exponential PL decay of the $MAPbI_3$/IDIC film was fitted with a decay time of 9.7 ns. Both PL and TRPL analyses demonstrated that IDIC is an efficient electron acceptor for $MAPbI_3$.

Since IDIC combines excellent trap passivation and good electron extraction of $MAPbI_3$, the application of IDIC as the ETL is expected to yield high performance devices. Thus, to demonstrate its potential, we used $MAPbI_3$ made by a interdiffusion method[41] with solvent annealing treatments[42] as the active layers and IDIC as a trap-passivation and ETL to fabricate p–i–n perovskite solar cells with a device structure (**Figure 5**a) of indium tin oxide (ITO)/poly(triaryl amine) (PTAA)/$MAPbI_3$/IDIC/C60/bathocuproine (BCP)/Cu, where PTAA was chosen as the hole transporting layer because of the large perovskite grain sizes formed on the nonwetting surface of PTAA. The

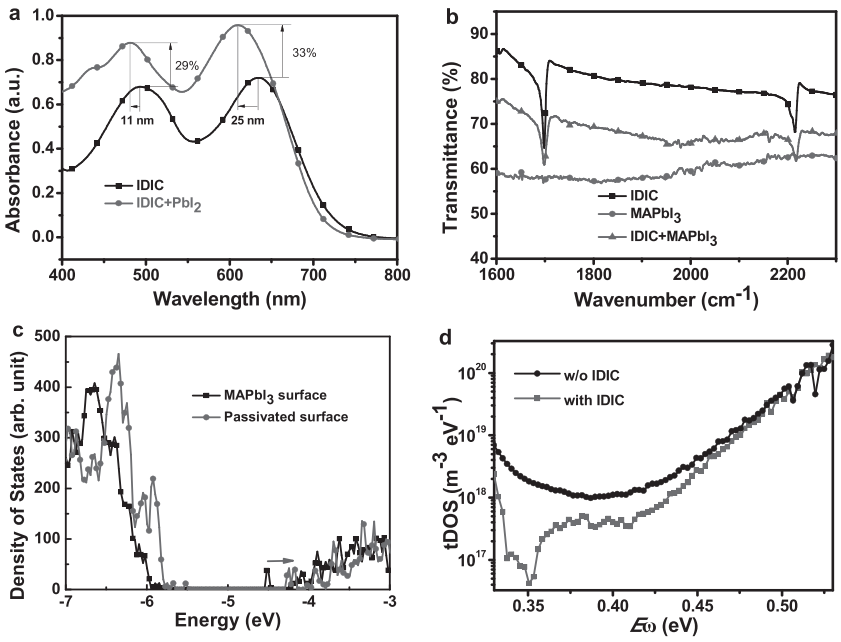

Figure 3. a) UV–vis absorption spectra of IDIC and IDIC: PbI_2 solutions; b) FTIR of the powder of IDIC, $MAPbI_3$, and IDIC: $MAPbI_3$ blend; c) computed density of states (DOS) of the PbI_2-terminated $MAPbI_3$ surface with Pb clusters, and with the passivated surface by the end group of IDIC; d) total DOS of $MAPbI_3$ based perovskite solar cells with and without (w/o) IDIC.

top-view (Figure S5, Supporting Information) and cross-section (Figure 5b) scanning electron microscopy (SEM) images show the grain sizes of $MAPbI_3$ is in the micrometer range. The grains connect the electrodes, and the GBs are perpendicular to the substrate for $MAPbI_3$ films to minimize the GB energy, which minimizes the charge recombination in the perovskite films. We characterized the morphology of the IDIC thin-film using optical microscope and SEM. Although as-cast IDIC has better molecular stacking than as-cast PCBM in the molecular scale, it is easy to form a continuous thin film on a perovskite surface by spin coating, as shown in optical (Figure S6, Supporting Information) and SEM images (Figure S7, Supporting Information). There were no "black dots" caused by self-aggregation on the surface of IDIC thin film. Due to the coverage of $MAPbI_3$ surface by less conductive IDIC, the GBs of the perovskite films in Figure S7 in the Supporting Information became misty compared with the uncoated $MAPbI_3$ film shown in Figure S5 in the Supporting Information. This good IDIC coverage is important for complete trap-passivation effect in the perovskite devices. The $MAPbI_3$/IDIC-based solar cells yield a high V_{OC} of 1.11 V and short-circuit density (J_{SC}) of 22.96 mA cm^{-2}, as well as a PCE of 19.5% (Figure 5c). Also we enlarged the device area from 7.5 to 12 mm^2 (Figure S8, Supporting Information), and no obvious difference in device performance was found. In contrast, the devices without IDIC layers between the $MAPbI_3$ and IDIC layers exhibit a lower V_{OC} of 1.03 V and J_{SC} of 19.37 mA cm^{-2}, and then a PCE of 13.5%; the enhanced V_{OC} and J_{SC} of $MAPbI_3$/IDIC-based perovskite solar cells can be attributed to efficient trap passivation and electron excitation of IDIC, respectively. Furthermore, compared with the typical PCBM-passivated perovskite solar cells with PCEs of 17%–18% in our previous reports,[15,43] perovskite solar cells with as-cast IDIC layers not only show better device PCEs, but also avoid the thermal annealing process, which may be attributed to the lower activation energy of the chemical reaction between the Lewis acid and base. The simple low temperature solution process without any extra thermal treatment simplifies the fabrication process and lowers the cost. For comparison, $MAPbI_3$/IDIC based solar cells have comparable PCEs and V_{OC} with those devices with insulating polymer layers as tunneling contact, where the thickness-sensitive insulating layers, such as polystyrene and Teflon etc., were inserted between the perovskite and the electron collection layer in perovskite solar cells to reduce charge recombination.[43] Figure 5d shows that the external quantum efficiency (EQE) spectrum of the devices with a IDIC layer is 20% higher than that of the control devices without IDIC. The photocurrent density calculated from EQE has <5% mismatch with those measured from *J–V* scanning. Statistic PCE distributions of 60 devices in Figure 5e, demonstrate the reliability and the repeatability of the performance enhancement by the IDIC passivation; over 70% of the devices with IDIC showed >16% PCEs. Figure 5f shows the steady photocurrent and PCE measured at the maximum power output point of the most efficient devices with and without IDIC, respectively. We recently demonstrated that ion migration at GBs plays a dominant role in causing photocurrent hysteresis.[44–46] Any material which can block the ion migration channel at grain boundaries is expected to eliminate the photocurrent hysteresis.[43] The steady photocurrent, stabilized PCE of $MAPbI_3$/IDIC based solar cells measured at the maximum power point agrees well with that measured from *J–V* scanning, excluding the existence of photocurrent hysteresis in our devices and confirming the accuracy of our device efficiency characterization. The absence of obvious photocurrent hysteresis of these devices is also confirmed by changing the photocurrent scanning directions (Figure S9, Supporting Information), which may be attributed to the penetration

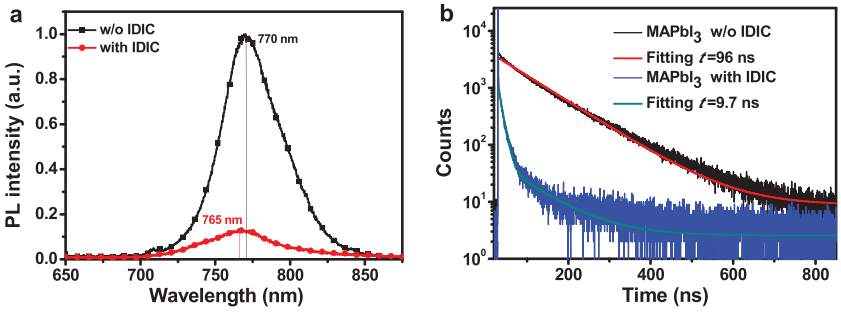

Figure 4. a) Steady PL and b) TRPL spectrum of $MAPbI_3$, and $MAPbI_3$/IDIC.

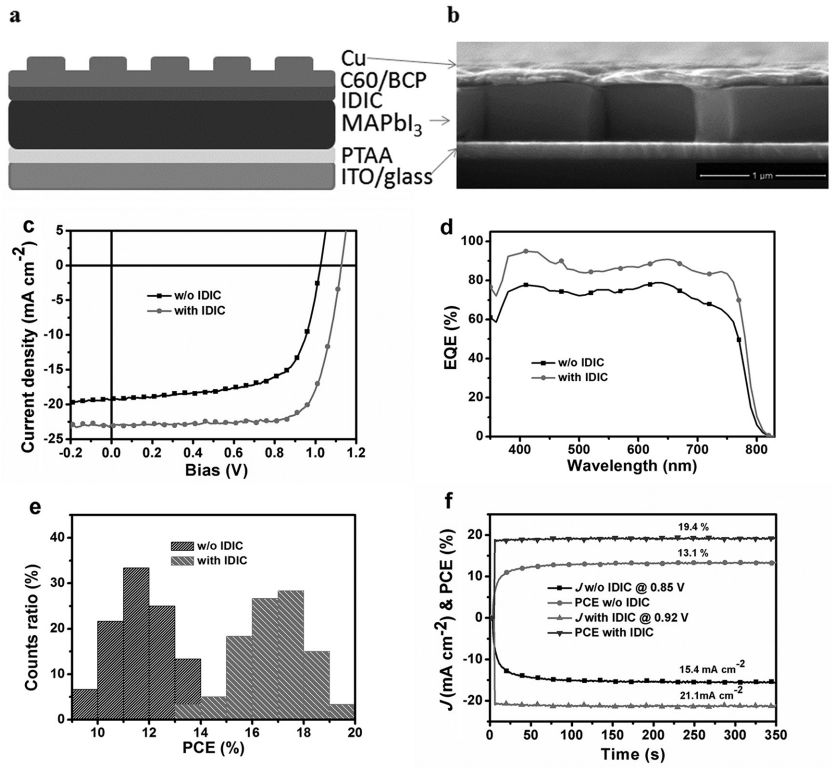

Figure 5. a) Device structure diagram and b) cross-section SEM image of ITO/PTAA/$MAPbI_3$/IDIC/C60/BCP/Cu; c) *J–V* curve, d) EQE, e) the statistics of PCE distribution, and f) steady-state measurement of J_{SC} and PCE of perovskite solar cells with and without IDIC.

of solution-processed IDIC into the GBs of $MAPbI_3$ to block the ion migration. In contrast, the perovskite solar cell without IDIC showed a steady output PCE of 13.1%, which is lower than that calculated from *J–V* scanning (13.5%). Meanwhile, during the first 60 s at the AM 1.5 G illumination, the device without IDIC shows a slight increase of the J_{SC} and PCE, which indicates the ion migration at GBs is not efficiently inhibited. Furthermore, perovskite solar cells with IDIC have good stability when stored under a dry inert atmosphere as shown in Figure S10 in the Supporting Information. After storage for 30 d, the device PCE with IDIC keeps almost stable around 90% of original value, which is better than that (≈80%) of the control devices without IDIC layer.

In conclusion, we introduced a π-conjugated Lewis base (IDIC) into perovskite solar cells as an interlayer between the perovskite and the cathode. The IDIC can extract electrons from perovskite layers because of its n-type semiconducting property, meanwhile the Lewis base end groups of IDIC can passivate the traps on the perovskite films at room temperature. $MAPbI_3$/IDIC based solar cells yielded a 45% PCE enhancement relative to the control perovskite solar cells without IDIC. This study also points to a new route to design interlayer materials based on new π-conjugated Lewis bases by combing various organic π-conjugated structures (e.g., aromatic fused-rings, oligothiophenes, etc.) and some typical Lewis base substituent groups (e.g., thiocyanato, sulfhydryl, etc.); and then π-conjugated Lewis bases can be broadly applicable to highly efficient perovskite solar cells with no hysteresis and stable power output, and many other high-performance optoelectronic applications, such as ultrafast photodetectors, lasers, and light-emitting diodes.

Experimental Section

The Fabrication and Measurement of Solar Cells: The methods of cleaning the ITO glass, the MAI synthesis[19] and the IDIC synthesis[33] can be found in the literature. The spin coating process was conducted in glovebox with an oxygen level lower than 100 particle per million (PPM). The PTAA was dissolved in toluene with a concentration of 2 mg mL^{-1}, and spin coated on the ITO/glass substrates at the speed of 5000 rpm. The spun PTAA films were thermally annealed at 100 °C for 10 min. The perovskite films were made by a interdiffusion method, where lead iodide (PbI_2) and MAI solutions were sequentially spun onto the substrates, followed by a thermal annealing driven diffusion process. The concentration of PbI_2 and MAI was 650 mg mL^{-1} in DMF and 65 mg mL^{-1} in isopropanol, respectively. The spun films were annealed at 100 °C for 60 min on hotplate under the cover of a glass petri dish. 20 μL DMF solvent was added at the edge of the petri dish during annealing process. After annealing, IDIC were deposited on top of $MAPbI_3$ by solution spin coating from a chloroform solution (2 mg mL^{-1}) at a speed of 6000 rpm. After the deposition of the IDIC layer, a 20 nm thickness of C60 was thermally evaporated with a deposition rate of 0.5 Å s^{-1}. The devices were finished by the evaporation of 8 nm BCP and 80 nm Cu electrode. The devices area was defined as the overlap of ITO and Cu electrode. The device area was 7.5–12 mm^2. The photocurrent–voltage (*J–V*) curves of the devices were measured in a glovebox with an oxygen level below 100 PPM. AM 1.5G irradiation (100 mW cm^{-2}) with a xenon–lamp-based solar simulator (Oriel 67005, 150W Solar Simulator) was used as the illumination source. A Schott visible-color glass-filtered (KG5 color-filtered) Si diode (Hamamatsu S1133) was used to calibrate the light intensity before photocurrent measurement. Keithley 2400 Source-Meter was used for recording the *J–V* measurement. Unless stated otherwise, the scanning direction for *J–V* measurement was from positive bias to negative bias. The voltage scanning rate was 0.1 V s^{-1}. The EQE measurement was conducted in air without device encapsulation.

Supporting Information

Supporting Information is available from the Wiley Online Library or from the author.

Acknowledgements

J.H. and X.C.Z. thank the National Science Foundation (NSF) through the Nebraska Materials Research Science and Engineering Center (MRSEC) (Grant No. DMR-1420645) and an NSF EPSCoR Track 2 grant (OIA-1538893). X.Z. thanks the NSFC (21673011). W.M. thanks the NSFC (21504066). X-ray data was acquired at beamlines 7.3.3 at the Advanced Light Source, which is supported by the Director, Office of Science, Office of Basic Energy Sciences, of the U.S. Department of Energy under Contract No. DE-AC02-05CH11231.

Received: August 25, 2016
Revised: October 9, 2016
Published online: December 6, 2016

[1] A. Kojima, K. Teshima, Y. Shirai, T. Miyasaka, *J. Am. Chem. Soc.* **2009**, *131*, 6050.
[2] M. A. Green, A. Ho-Baillie, H. J. Snaith, *Nat. Photonics* **2014**, *8*, 506.
[3] J. H. Heo, S. H. Im, J. H. Noh, T. N. Mandal, C.-S. Lim, J. A. Chang, Y. H. Lee, H.-j. Kim, A. Sarkar, K. NazeeruddinMd, M. Gratzel, S. I. Seok, *Nat. Photonics* **2013**, *7*, 486.
[4] M. M. Lee, J. Teuscher, T. Miyasaka, T. N. Murakami, H. J. Snaith, *Science* **2012**, *338*, 643.
[5] H. J. Snaith, *J. Phys. Chem. Lett.* **2013**, *4*, 3623.
[6] X. Li, D. Bi, C. Yi, J.-D. Décoppet, J. Luo, S. M. Zakeeruddin, A. Hagfeldt, M. Grätzel, *Science* **2016**, *353*, 58.
[7] W. Chen, Y. Z. Wu, Y. F. Yue, J. Liu, W. J. Zhang, X. D. Yang, H. Chen, E. B. Bi, I. Ashraful, M. Gratzel, L. Y. Han, *Science* **2015**, *350*, 944.
[8] Q. Dong, Y. Fang, Y. Shao, P. Mulligan, J. Qiu, L. Cao, J. Huang, *Science* **2015**, *347*, 967.
[9] D. Shi, V. Adinolfi, R. Comin, M. Yuan, E. Alarousu, A. Buin, Y. Chen, S. Hoogland, A. Rothenberger, K. Katsiev, Y. Losovyj, X. Zhang, P. A. Dowben, O. F. Mohammed, E. H. Sargent, O. M. Bakr, *Science* **2015**, *347*, 519.
[10] S. De Wolf, J. Holovsky, S.-J. Moon, P. Löper, B. Niesen, M. Ledinsky, F.-J. Haug, J.-H. Yum, C. Ballif, *J. Phys. Chem. Lett.* **2014**, *5*, 1035.
[11] J. Huang, Y. Shao, Q. Dong, *J. Phys. Chem. Lett.* **2015**, *6*, 3218.
[12] H. Wei, Y. Fang, P. Mulligan, W. Chuirazzi, H.-H. Fang, C. Wang, B. R. Ecker, Y. Gao, M. A. Loi, L. Cao, J. Huang, *Nat. Photonics* **2016**, *10*, 333.
[13] Y. Fang, Q. Dong, Y. Shao, Y. Yuan, J. Huang, *Nat. Photonics* **2015**, *9*, 679.
[14] B. Wu, H. T. Nguyen, Z. Ku, G. Han, D. Giovanni, N. Mathews, H. J. Fan, T. C. Sum, *Adv. Energy Mater.* **2016**, *6*, 1600551.
[15] C. Bi, Q. Wang, Y. Shao, Y. Yuan, Z. Xiao, J. Huang, *Nat. Commun.* **2015**, *6*, 7747.
[16] H. Zhou, Q. Chen, G. Li, S. Luo, T.-b. Song, H.-S. Duan, Z. Hong, J. You, Y. Liu, Y. Yang, *Science* **2014**, *345*, 542.
[17] B. Yang, O. Dyck, J. Poplawsky, J. Keum, A. Puretzky, S. Das, I. Ivanov, C. Rouleau, G. Duscher, D. Geohegan, K. Xiao, *J. Am. Chem. Soc.* **2015**, *137*, 9210.
[18] W. S. Yang, J. H. Noh, N. J. Jeon, Y. C. Kim, S. Ryu, J. Seo, S. I. Seok, *Science* **2015**, *348*, 1234.
[19] Z. Xiao, Q. Dong, C. Bi, Y. Shao, Y. Yuan, J. Huang, *Adv. Mater.* **2014**, *26*, 6503.
[20] Y. Shao, Z. Xiao, C. Bi, Y. Yuan, J. Huang, *Nat. Commun.* **2014**, *5*, 5784.
[21] J. Xu, A. Buin, A. H. Ip, W. Li, O. Voznyy, R. Comin, M. Yuan, S. Jeon, Z. Ning, J. J. McDowell, P. Kanjanaboos, J.-P. Sun, X. Lan, L. N. Quan, D. H. Kim, I. G. Hill, P. Maksymovych, E. H. Sargent, *Nat. Commun.* **2015**, *6*, 7081.
[22] N. K. Noel, A. Abate, S. D. Stranks, E. S. Parrott, V. M. Burlakov, A. Goriely, H. J. Snaith, *ACS Nano* **2014**, *8*, 9815.
[23] A. Abate, M. Saliba, D. J. Hollman, S. D. Stranks, K. Wojciechowski, R. Avolio, G. Grancini, A. Petrozza, H. J. Snaith, *Nano Lett.* **2014**, *14*, 3247.
[24] D. W. de Quilettes, S. M. Vorpahl, S. D. Stranks, H. Nagaoka, G. E. Eperon, M. E. Ziffer, H. J. Snaith, D. S. Ginger, *Science* **2015**, *348*, 683.
[25] C. Bi, Y. Shao, Y. Yuan, Z. Xiao, C. Wang, Y. Gao, J. Huang, *J. Mater. Chem. A* **2014**, *2*, 18508.
[26] A. Dualeh, N. Tétreault, T. Moehl, P. Gao, M. K. Nazeeruddin, M. Grätzel, *Adv. Funct. Mater.* **2014**, *24*, 3250.
[27] Q. Chen, H. Zhou, T.-B. Song, S. Luo, Z. Hong, H.-S. Duan, L. Dou, Y. Liu, Y. Yang, *Nano Lett.* **2014**, *14*, 4158.
[28] W.-J. Yin, T. Shi, Y. Yan, *Appl. Phys. Lett.* **2014**, *104*, 063903.
[29] F. Deschler, M. Price, S. Pathak, L. E. Klintberg, D.-D. Jarausch, R. Higler, S. Hüttner, T. Leijtens, S. D. Stranks, H. J. Snaith, M. Atatüre, R. T. Phillips, R. H. Friend, *J. Phys. Chem. Lett.* **2014**, *5*, 1421.
[30] K. Wojciechowski, T. Leijtens, S. Siprova, C. Schlueter, M. T. Hörantner, J. T.-W. Wang, C.-Z. Li, A. K. Y. Jen, T.-L. Lee, H. J. Snaith, *J. Phys. Chem. Lett.* **2015**, *6*, 2399.
[31] Y. Li, Y. Zhao, Q. Chen, Y. Yang, Y. Liu, Z. Hong, Z. Liu, Y.-T. Hsieh, L. Meng, Y. Li, *J. Am. Chem. Soc.* **2015**, *137*, 15540.
[32] Z. Zhu, C.-C. Chueh, F. Lin, A. K. Y. Jen, *Adv. Sci.* **2016**, *3*, 1600027.
[33] Y. Z. Lin, Q. He, F. W. Zhao, L. J. Huo, J. Q. Mai, X. H. Lu, C. J. Su, T. F. Li, J. Y. Wang, J. S. Zhu, Y. M. Sun, C. R. Wang, X. W. Zhan, *J. Am. Chem. Soc.* **2016**, *138*, 2973.
[34] D. M. Smilgies, *J. Appl. Crystallogr.* **2009**, *42*, 1030.
[35] Y. Shao, Y. Yuan, J. Huang, *Nat. Energy* **2016**, *1*, 15001.
[36] R. G. Pearson, *Science* **1966**, *151*, 172.
[37] A. W. Adamson, W. L. Waltz, E. Zinato, D. W. Watts, P. D. Fleischauer, R. D. Lindholm, *Chem. Rev.* **1968**, *68*, 541.
[38] T. Walter, R. Herberholz, C. Müller, H. W. Schock, *J. Appl. Phys.* **1996**, *80*, 4411.
[39] C. Melzer, E. J. Koop, V. D. Mihailetchi, P. W. M. Blom, *Adv. Funct. Mater.* **2004**, *14*, 865.
[40] J. A. Carr, S. Chaudhary, *Energy Environ. Sci.* **2013**, *6*, 3414.
[41] Z. Xiao, C. Bi, Y. Shao, Q. Dong, Q. Wang, Y. Yuan, C. Wang, Y. Gao, J. Huang, *Energy Environ. Sci.* **2014**, *7*, 2619.
[42] Z. G. Xiao, Q. F. Dong, C. Bi, Y. C. Shao, Y. B. Yuan, J. S. Huang, *Adv. Mater.* **2014**, *26*, 6503.
[43] Q. Wang, Q. Dong, T. Li, A. Gruverman, J. Huang, *Adv. Mater.* **2016**, *28*, 6734.
[44] Y. Shao, Y. Fang, T. Li, Q. Wang, Q. Dong, Y. Deng, Y. Yuan, H. Wei, M. Wang, A. Gruverman, J. E. Shield, J. Huang, *Energy Environ. Sci.* **2016**, *9*, 1752.
[45] Y. Yuan, J. Huang, *Acc. Chem. Res.* **2016**, *49*, 286.
[46] Z. G. Xiao, Y. B. Yuan, Y. C. Shao, Q. Wang, Q. F. Dong, C. Bi, P. Sharma, A. Gruverman, J. S. Huang, *Nat. Mater.* **2015**, *14*, 193.